Reduced Frequency and Power Spectra of Wind Pressure of a Tall Building Having "Z" Shape in Plan

Rajdip Paul (rajdippaul87@gmail.com)
Hooghly Engineering & Technology College
Sujit Kumar Dalui
Indian Institute of Engineering Science and Technology, P.O.- Botanic Garden

Research Article

Keywords: Tall building, CFD, Vortex shedding, Peak pressure, Reduced Frequency, Power Spectral Density

Posted Date: May 9th, 2022

DOI: https://doi.org/10.21203/rs.3.rs-1618818/v1

Reduced Frequency and Power Spectra of Wind Pressure of a Tall Building Having "Z" Shape in Plan

Rajdip Paul*[1a] and Sujit Kumar Dalui[2b]

1. Assistant Professor, Civil Engineering Department, Hooghly Engineering & Technology College, Vivekananda Road, Pipulpati Post, Chinsurah, West Bengal-712103, Hooghly, India,
2. Assistant Professor, Civil Engineering Department, Indian Institute of Engineering Science and Technology, Shibpur, P.O.- Botanic Garden, Shalimar, West Bengal-711103, Howrah, India

Abstract. This study envisages a tall building model's dynamic behaviour with a 'Z' shape in plan and exposed to cyclonic wind tested using numerical simulation technique. The computational Fluid Dynamics (CFD) simulation tool of $ANSYS - CFX$ is adopted in the present study. The geometric scale is considered as 1:300, whereas the velocity scale is taken to be 1:5. Wind streamlines under different wind occurrence angles on the building are displayed perceptibly, ensuring vortex shedding at the region of disturbed flow where the wind suction and pressure amalgamates. The peak wind pressures and suctions at building facets are presented under different wind angles. Again the features of normalized power spectra of wind pressure at the top part, main body, and bottom part of the building subjected to wind azimuths ranging from $0°$ to $150°$ are presented. It is found that at the bottom part of the building, the peak values of standardized power spectra occur in the low-frequency range, although, at the top part and main body of the building, the vortex shedding energy intensifies at relatively high reduced frequencies. The determination of reduced frequency is of paramount importance to evade resonance under wind tempted shakings of soaring buildings.

Keywords Tall building; CFD; Vortex shedding; Peak pressure; Reduced Frequency; Power Spectral Density

* Corresponding author
[a] Ph.D., E-mail: rajdippaul87@gmail.com, ORCID ID: 0000-0001-9514-8478
[b] Ph.D., E-mail: sujit.dalui@gmail.com, ORCID ID: 0000-0002-3593-4837

1. Introduction

Tall flexible buildings are susceptible to vibrate in space with high frequency under lateral load and shall be scrutinized to determine wind-tempted swaying or excitations in along-wind and crosswind directions. As per IS 875 (Part 3): 2015 [1], buildings and structures with cladding shall be studied for dynamic wind effects when the building height to least lateral dimension ratio is greater than 5 or if the natural frequency of a building in the first vibration mode is below 1.0 Hz. Due to the intricacy of the dynamic reactions, experimental methods using wind tunnels and numerical techniques under replicated atmospheric boundary layers are the solitary feasible means of finding exact wind design parameters [2, 3]. Besides, if the plan or elevation of the tall building is unusual, then wind-structure interaction becomes even more complicated due to inertial coupling [4].

Researchers in wind engineering carried out past studies to get correct information about wind pressures and forces on tall structures. Kareem (1987) exemplified the effects of vicinity and interference on prismatic bluff bodies' dynamic reactions [5]. Saatoff and Melbourne (1989) performed an experimental analysis to analyze substantial negative peak pressures near sharp bluffs' leading edge [6]. Stathopoulos et al. (1991) employed a wind tunnel model experiment to obtain local pressure coefficients considering the effect of roof slope and the number of spans for multi-span gabled roofs [7]. Melbourne (1993) studied the shear layers' behavior, unraveling the leading edge of the bluff body. The author also attributed the critical position of turbulence, particularly the impact on the pressures under the shear layer's reattachment [8]. Surry and Djakovich (1995) studied high peak wind suctions built on building models, their dependence on building form and approaching simulated atmospheric shear flow characteristics [9]. T. Kijewski and Kareem (2001) put forward a wind tunnel test to foresee the responses in the along-wind, crosswind, and torsional directions. The study presented measured power spectra and a comparison among the response anticipated by the wind tunnel test and that assessed by international codes [10]. Analytical expressions were recommended by Liang et al. (2004) to determine various sorts of wind tempted dynamic responses, specifically in torsional directions [11]. Lin et al. (2004) conferred that the crosswind and torsional responses surpass the along-wind response for super high-rise buildings [12]. Balendra et al. (2005) discussed the details and test results of the laser positioning measurement technique of wind-tempted displacements in a high-rise building, and also comparison has been made with the outcomes obtained from the conventional strain gauge method [13]. Gomes et al. (2005) presented wind design parameters for U and L-shaped in plan building models considering a 1:100 length scale [14]. Along with structural safety, Irwin (2007) gave due importance to the serviceability criteria like occupant comfort under dynamic wind occurrence [15]. The author studied many

bluff body aerodynamic occurrences to get a deep insight into structural safety and occupant comfort. The features of boundary layer and storm reaction were studied by Fu et al. (2008) for two high buildings. The study adopted the field measurements technique [16]. Kim et al. (2008) conferred the taper ratios and the damping ratio's effects on decreasing the crosswind excitations of high-rise buildings by progressively reduced velocity [17]. Zhang and Gu (2008) studied wind-tempted interference effects by experimenting in a low-speed wind tunnel, having a staggered arrangement of two square buildings with several oblique wind incidence angles. The results are compared with numerical simulation also [18]. Kwok et al. (2009) reviewed occupants' perception of vibration and tolerance thresholds in high-rise buildings under dynamic wind effects [19]. Tse et al. (2009) varied the size of recessed and chamfered corners of high-rise buildings being square in plan and deliberated the general concept of determining wind loads and reactions [20]. Gu and Xie (2010) illustrated interference effects on the peak and mean wind pressure of two and three high-rise buildings configuration considering dynamic-wind response [21]. Bhatnagar et al. (2012) discussed the outcomes of a study on a low-rise building model with a saw-tooth roof carried out in an open circuit wind tunnel [22]. Amin and Ahuja (2013) considered different side ratios on rectangular plan-shaped tall buildings and carried out wind tunnel experiments. The study kept the height and area the same for all models, varied the wind incidence from 0º to 90º at an interval of 15º, and presented the wind pressure coefficients for each case [23]. The deviation of pressure dispersal of a tall square plan-shaped building for various wind azimuths was studied by Verma et al. (2013) through a boundary layer wind tunnel study [24]. The data thus acquired facilitates the design of the structural frame and its cladding unit. Muehleisen and Patrizi (2013) considered depth to height ratio, depth to breadth ratio, and angle of wind attack as independent variables for developing parametric equations to predict pressure coefficients on the facets of rectangular low-rise building models conducting wind tunnel experiments [25]. Kushal et al. (2013) discussed the significance of the building's plan shape in wind pressure [26]. Dagnew and Bitsuamlak (2014) evaluated wind-tempted aerodynamic forces on a standard high-rise building using the LES (large-eddy simulation) method [27]. Sun and Gu (2014) applied a simultaneous numerical solution concerning a linear elastic model to observe the FSI (fluid-structure interaction) of membrane structures subjected to wind actions [28]. Huang et al. (2014) observed the features of amplitudes and wind forces power spectra along X, Y, and RZ axes considering a 492 m tall building with a varied section along with the altitude. The authors adopted wind tunnel tests (rigid model) and proposed analytical expressions to obtain along-wind, crosswind, and torsional wind force power spectra in varying wind directions [29]. The mean surface pressure dissemination on the walls of an 'E' plan-shaped tall building was scrutinized by Bhattacharyya et al. (2014) through analytical studies validated with experimental outcomes for

a widespread wind occurrence angle [30]. Zhi et al. (2015) developed a Kalman filtering-based inverse approach to estimate the wind loads on super-high-rise buildings based on limited structural responses [31]. Paul and Dalui (2016) numerically investigated the external wind pressure coefficients and wind force coefficients' variation on a 'Z' shaped in plan tall building for a wind range of wind incidences. For numerical simulation, the Computational Fluid Dynamics package of $ANSYS$ was used in the study [32]. Sanyal et al. (2018) focused on the variation of pressure due to the courtyard's presence and opening of a rectangular plan-shaped building numerically, and further polynomial regression analysis is performed to evaluate the pressure coefficients for any wind direction [33]. Li et al. (2018) studied the effect of horizontal changes such as corner-cutting on high-rise buildings [34]. Mallick and Mohanta (2019) carried out wind tunnel model experiments to feed GMDH neural network for developing equations for the prognosis of average external pressure coefficients on the facets of various C plan-shaped buildings [35]. Off late, artificial neural networks are adopted to present the average pressure coefficients on all building facets of setback high-rise buildings (Bairagi and Dalui, 2020) and cross-plan-shaped high-rise buildings (Paul and Dalui, 2020) [36, 37]. Paul and Dalui (2021) further utilized artificial neural networks to compare the along and crosswind force coefficients obtained using CFD and parametric equations [38].

The current study is carried out to understand the dynamics in the behaviour of wind-tempted responses of a tall building 'Z' shaped in the plan under different wind azimuths. The 'Z' shape is preferred because it is a popular shape in buildings like hospitals, airports, academic blocks, and hostels [39]. The outcomes of the present study apply to any rectangular building with wings having a similar aspect ratio and in-plan ratio. The aspect ratio for the present study is 1:2 (width: height), and the in-plan ratio is 1:1. Therefore, the results can be used suitably adopted for any such practical building. Transient analysis is performed using the numerical simulation technique, and the characteristics of normalized power spectra of wind pressure at some crucial measurement levels of altitude are analyzed and presented in this study. The short-term static wind effects may be characterized by a wind response spectrum, i.e., the wind response's power spectral density [40]. Wind pressure's power spectral densities express the way energy induced by the wind pressure in a definite point in space is dispersed between different frequencies. The vortex shedding frequencies can be obtained from the power spectra of wind pressures, and it should be ensured that the natural frequency of the building does not coincide. So, the resonance phenomenon leading to abnormally high amplitudes of vibration can be avoided.

2. The parametric model and algorithm of the research

The rigid model geometric scale is taken as 1:300. The clear dimension of the length and width of each wing is 100 and 50 mm, respectively, as shown in Fig. 1. The building has a 22500 mm^2 plan area and 500 mm overall height. Building wings are at an angle of 90^{o} with a rectangular body. The three-dimensional view of the study building is depicted in Fig. 2.

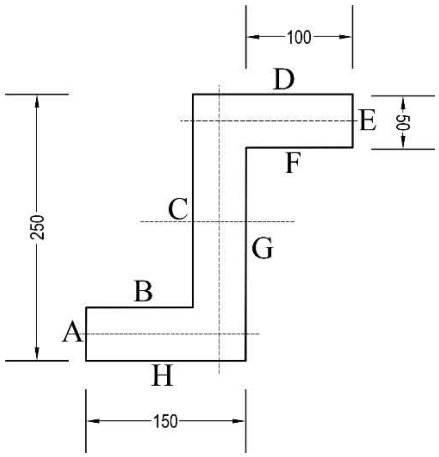

Fig. 1 The study building in plan (Unit: "mm")

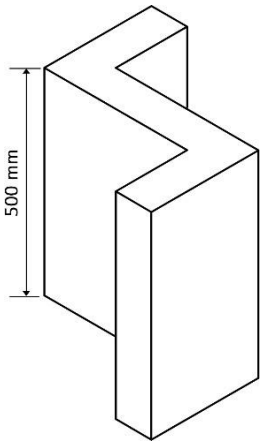

Fig. 2 The study building in isometric

Fig. 3 illustrates the algorithm of the present study. Initially, the research aims to identify and then the shape of the study building is selected. $ANSYS - CFX$ is used for the numerical simulation with RANS k-ε turbulence modeling. The details of the domain, meshing, and necessary boundary conditions of the CFD are defined. The calibration of the adopted CFD technique is indispensable, and it is done using the provisions of international standards of wind load for a square-shaped building. After suitable calibration, the CFD is utilized to implement dynamic-wind analysis for the proposed building model under critical wind angles. Wind streamlines are generated after processing the simulation results to present the wind flow characteristics. Finally, the normalized power spectra of wind pressure against reduced frequency are plotted for the building surfaces under different wind occurrence angles.

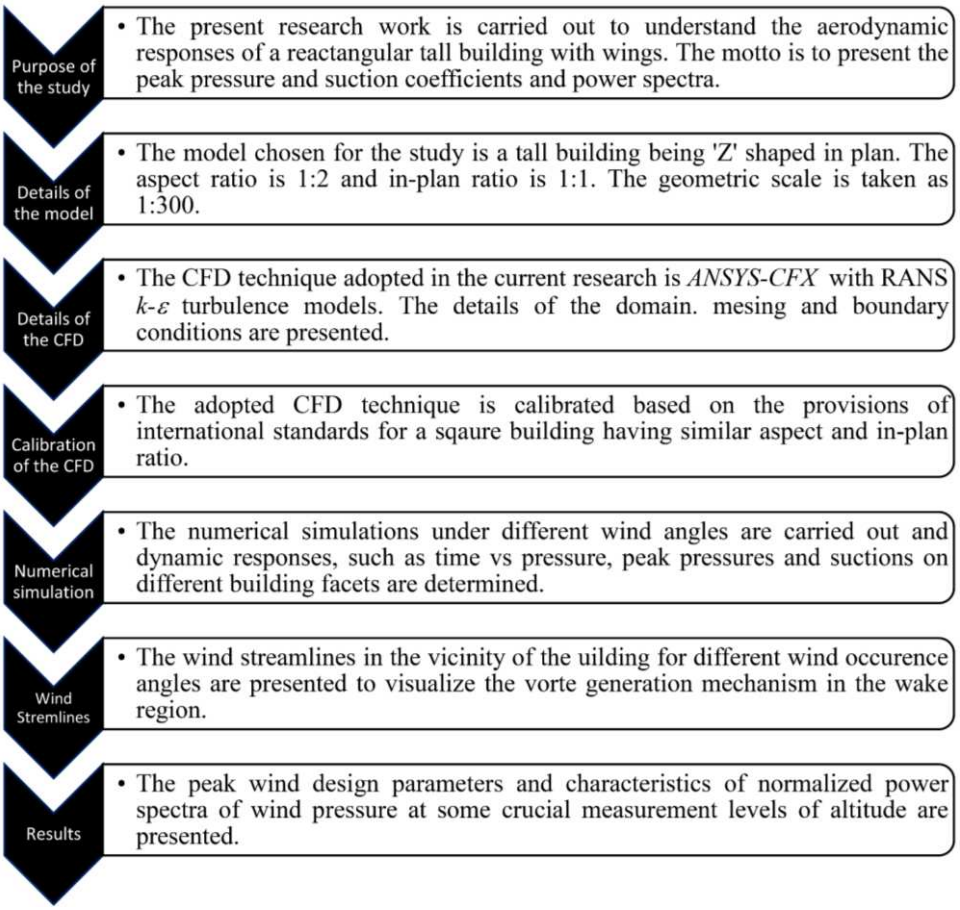

Fig. 3 The algorithm of the present research

3. Details of the numerical simulation technique

As deliberated in section 2, RANS $k-\varepsilon$ turbulence modeling is adopted for the current study. During calibration of the CFD technique, as discussed in sub-section 3.4, three different turbulence models namely $k-\varepsilon$, $k-\omega$, and SST were adopted. An excellent match was observed with the standard design parameters for the $k-\varepsilon$ model and used for the actual study. Kinetic energy and eddies dissipation in the turbulence are defined by 'k' and 'ε' respectively. The building is taken as a bluff body, and wind streams near the building are studied to visualize the vortices generation at the wake region. Turbulent flows in RANS models are demarcated by the standard equations of continuity and momentum, termed after Navier and Stokes, modified to the following Equation (1) and (2).

$$\frac{\partial \rho}{\partial t} + \frac{\partial}{\partial x_j}(\rho \mathrm{U_j}) = 0 \qquad (1)$$

$$\frac{\partial \rho U_i}{\partial t} + \frac{\partial}{\partial x_j}(\rho \mathrm{U_i U_j}) = \frac{\partial \acute{P}}{\partial x_i} + \frac{\partial}{\partial x_j}\left[\mu_{eff}\left(\frac{\partial U_i}{\partial x_j} + \frac{\partial U_j}{\partial x_i}\right)\right] + S_M \qquad (2)$$

Where 'p', μ_{eff} and S_M are modified pressure, effective turbulence viscosity, and the sum of the body forces, respectively. The $k-\varepsilon$ turbulence model is based on the eddy viscosity notion and therefore analogous to the zero equation model. Hence,

$$\mu_{eff} = \mu + \mu_t \tag{3}$$

In equation 3, μ_t is the viscosity of the turbulent flow. The $k-\varepsilon$ model undertakes that μ_t is connected to the k and ε by the relation,

$$\mu_t = C_\mu \rho \frac{k^2}{\varepsilon} \tag{4}$$

The value of the constant C_μ is 0.09 whereas the value of k and ε is obtained from the following differential equations.

$$\frac{\partial(\rho k)}{\partial t} + \frac{\partial}{\partial x_j}(\rho \mathrm{U_j}\, \mathrm{k}) = \frac{\partial}{\partial x_j}\left[(\mu + \frac{\mu_t}{\sigma_k})\frac{\partial k}{\partial x_j}\right] + P_k - \rho\varepsilon + P_{kb} \tag{5}$$

$$\frac{\partial(\rho\varepsilon)}{\partial t} + \frac{\partial}{\partial x_j}(\rho \mathrm{U_j}\, \varepsilon) = \frac{\partial}{\partial x_j}\left[(\mu + \frac{\mu_t}{\sigma_\varepsilon})\frac{\partial \varepsilon}{\partial x_j}\right] + \frac{\varepsilon}{k}(\mathrm{C}_{\varepsilon 1} P_k - \mathrm{C}_{\varepsilon 2} + \mathrm{C}_{\varepsilon 1} P_{\varepsilon \mathrm{b}}) \tag{6}$$

The turbulence production caused by viscous forces, P_k, is modelled by:

$$P_k = \mu_t\left(\frac{\partial U_i}{\partial x_j} + \frac{\partial U_j}{\partial x_i}\right)\frac{\partial U_i}{\partial x_j} - \frac{2}{3}\frac{\partial U_k}{\partial x_k}(3\mu_t \frac{\partial U_k}{\partial x_k} + \rho k) \tag{7}$$

The value of the $k-\varepsilon$ turbulence model constants in $ANSYS\ CFX$, $\mathrm{C}_{\varepsilon 1}$, $\mathrm{C}_{\varepsilon 2}$, σ_k and σ_ε, are 1.44, 1.92, 1.00, and 1.30 respectively. The air density, ρ is taken as 1.224 kg/m^3. Low turbulence intensity in the setup of *ANSYS-CFX* modeling is taken corresponds to 1% turbulence. The wind speed is taken as 10 m/s near the inlet. This is because the study's basic wind velocity is considered 50 m/s, and the velocity scale is 1:5.

3.1 Domain and meshing used in computational fluid dynamics

The precision of a CFD technique primarily depends on the domain size and the grid pattern chosen for the numerical simulation. The computational domain shall be such that the vortex generation in the wake zone is entirely assimilated. Considering 'H' is the building's altitude, as per the guidelines provided by Revuz et al. [41], 5H, 15H, 5H, and 5H clearances are provided at the upstream, downstream, side, and the top of the building, respectively. Revuz et al. varied the high-rise building's domain size and considered the accuracy in deriving the vortex generation and velocity fluctuations in the building's turbulent downstream. The domain adopted for the numerical simulation is presented in Fig. 4 (a)-(c).

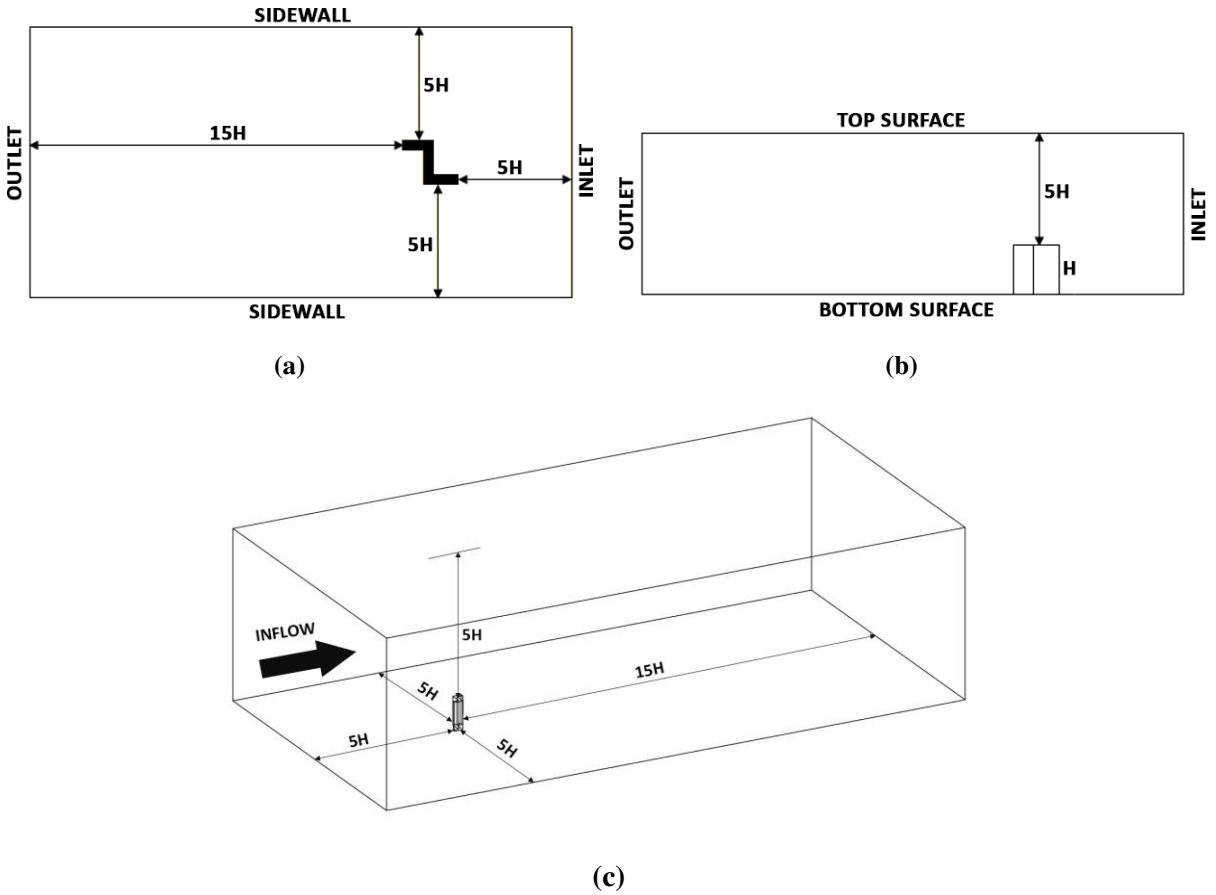

Fig. 4 Domain used for the study (a) Plan; (b) Elevation; (c) Isometric

A blend of hexagonal and tetrahedron meshing is used for meshing the building and the domain. More delicate meshing near the building is provided to accurately access the responses on the building's surfaces, while relatively coarser meshing with suitable y plus values in the remaining domain may ease the calculation time without hampering the accuracy of the results. The grid pattern adopted for the numerical simulation is presented in Fig. 5. An enlarged corner view of the building showing the mesh pattern is also shown in the figure.

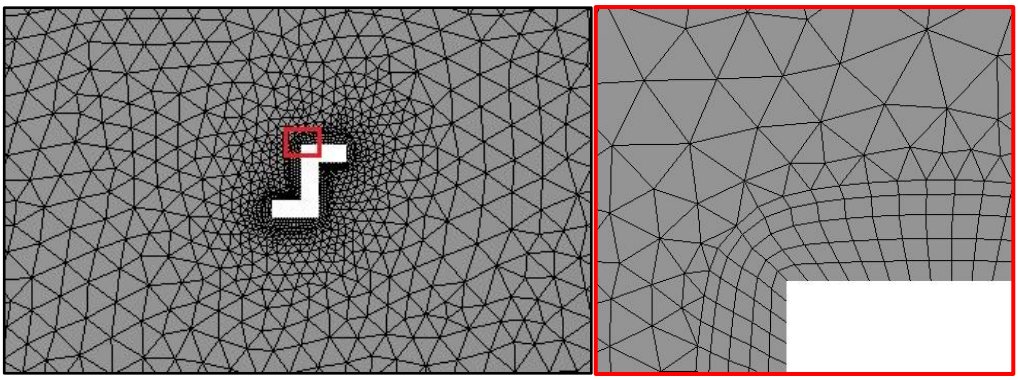

Fig. 5 Mesh pattern around the building and domain

3.2 Grid sensitivity test

The grid sensitivity test is an important criterion to conclude that additional lessening in grid size does not give better results. The grid sensitivity test is done by the hit and trial process reducing the grid size in the respective trial thereby increasing the number of volume elements within the domain. The test is done on the 'Z' shaped building under 0º wind incidence angle. The mesh pattern for the building model and the domain is generated six times in $ANSYS\ CFX - CFD$ adopting finer grids in subsequent trials. The face average external wind pressure coefficients for all the building faces as defined in section 2, are obtained in each trial. The results of the grid independence are plotted and presented in Fig. 6. It is essential to arrive at an optimum solution so that the accuracy and analysis time is balanced. Founded on the grid sensitivity test, as shown in Fig. 6, the optimum number of volume elements is acquired as 8.1×10^6 and the corresponding grid pattern is adopted for the rest of the study.

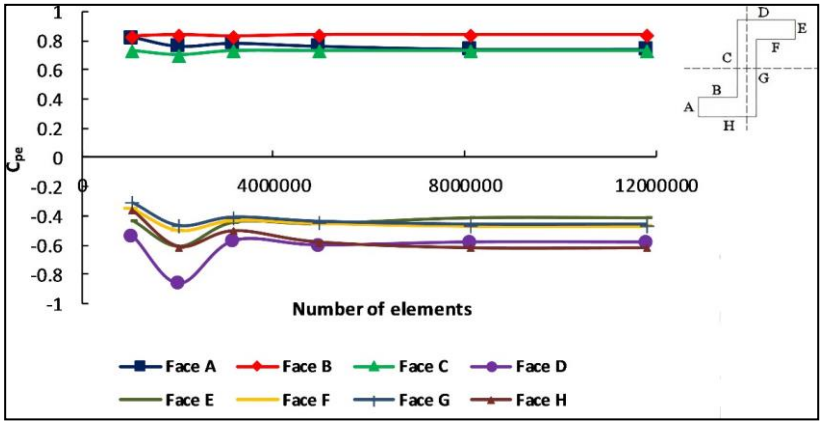

Fig. 6 The results of the grid independence test

3.3 Boundary conditions in CFD

CFD may be used as a suitable replacement for the wind tunnel experiment method if a high degree of similarity is achieved in both methods' boundary conditions, primarily for the inflow boundary. The turbulence intensity and the velocity profile along the altitude adjacent to the windward face are related to the experimental and numerical technique based on the results presented by Dalui, 2008 for a tall octagonal building [42]. In the numerical study, a power law is used with $\alpha = 0.133$ to generate the boundary layer wind stream imitating terrain category-II of $IS: 875\ (Part\ 3) - 2015$. Excellent matches are obtained in the comparative study, and it may be concluded that the boundary conditions used for the numerical study are nearly similar to the experimental method. The

comparison of the turbulence intensity and the velocity profile is presented in Fig. 7 (a) and (b), respectively. Moreover, the velocity spectrum for the current study at the incident plane of the 'Z' shaped model is compared with the Von Karman and Davenport spectrum in Fig. 8. It is seen that the velocity spectrum is reasonably in line with the standard spectra. Therefore, the study is producing the spectral content with sufficient accuracy also, an important aspect of tall buildings.

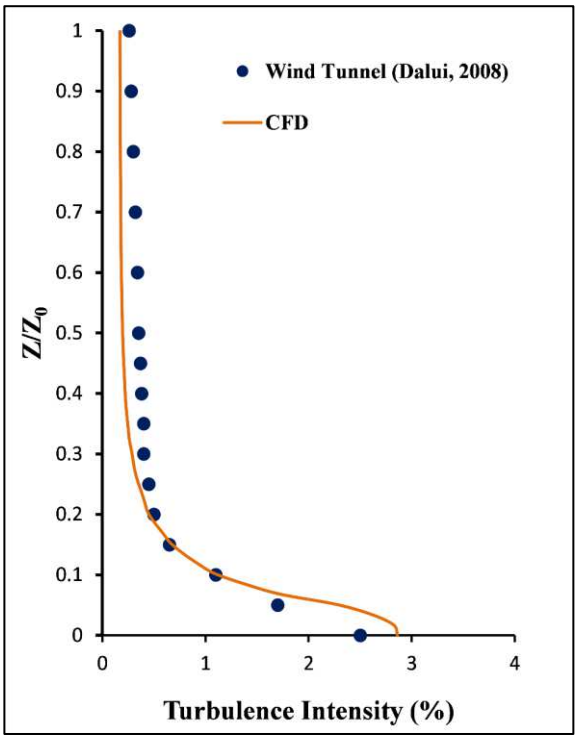

Fig. 7 (a) Turbulence intensity

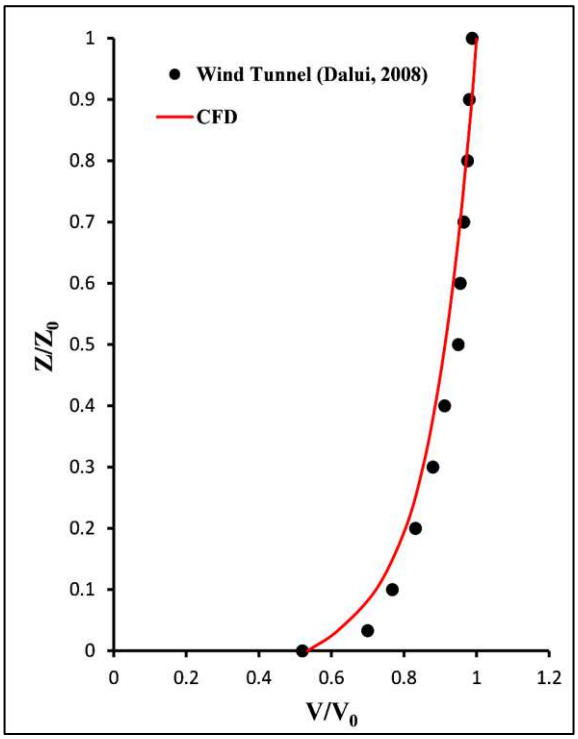

Fig. 7 (b) velocity profile

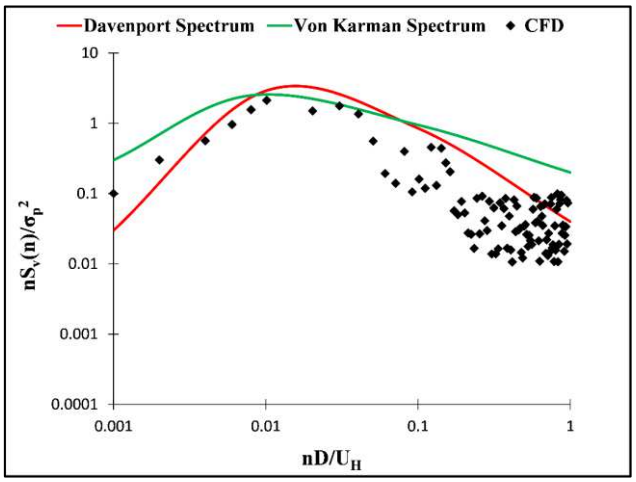

Fig. 8 Velocity spectrum at the incident plane as per CFD and standard spectra

3.4 Calibration of the CFD technique

The CFD technique is calibrated by evaluating external mean pressure coefficients (C_p) of the square high-rise building with an aspect ratio h/w=5. The results of CFD are compared with three international standards for the evaluation of wind load, namely $IS: 875(part-3): 2015$ [1], $AS-NZS\ 1170.2-2021$ [43], and $ASCE\ 7-16$ [44]. The results are presented in Table 3. An outstanding match is observed in the CFD results and the recommendations of the code AS-NZS 1170.2:2021 and ASCE 7-16. There is no deviation in the results obtained for the windward face of the building subjected to 0° wind angle of attack. Again for the sidewalls, the disparity is 14.3% and 7.7% concerning ASCE 7-16 and AS-NZS 1170.2:2021, respectively. However, for the leeward face, the outcome of CFD is differing 20% regarding both the standards. The trembling vortices produced in the wake zone are responsible for the deviance in the outcome.

Table 1 Comparison of C_{pe} on the facets of square building model

Building plan	Reference	$\frac{h}{w}$	Wind incidence (θ)	C_{pe}			
				Facet A	Facet B	Facet C	Facet D
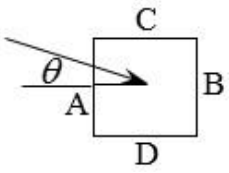	CFD	$\frac{h}{w}=5$	0°	+0.80	-0.40	-0.60	-0.60
			90°	-0.60	-0.60	+0.80	-0.40
	IS: 875 (Part 3) - 2015	$\frac{3}{2}<\frac{h}{w}<6$	0°	+0.80	-0.25	-0.80	-0.80
			90°	-0.80	-0.80	+0.80	-0.25
	AS-NZS 1170.2:2021	Any $\frac{h}{w}$	0°	+0.80	-0.50	-0.65	-0.65
			90°	-0.65	-0.65	+0.80	-0.50
	ASCE 7-16	Any $\frac{h}{w}$	0°	+0.80	-0.50	-0.70	-0.70
			90°	-0.70	-0.70	+0.80	-0.50

4. Results and discussions

The transient wind analysis is carried out for the proposed building using the numerical simulation tool of *ANSYS-CFX*. The domain, meshing, turbulence intensity, and velocity profile used for the purpose are discussed in the preceding sections. The definition of the building surfaces along with the wind azimuths is shown in Fig. 9. The

wind angles are considered from 0º to 150º with an increment of 30º. Transient wind analysis is carried out in the numerical simulation study using 3D URANS models. Total gauging time is taken as 6 s with a maximum time step of 0.01 s in every simulation. Therefore, the total number of time steps is 600 per simulation. Aerodynamic effects on the building at 0º and 180º being the same, wind angle up to 150º are considered for the present research. Though the results can be better presented if the increment in wind angle is further reduced, a 30º increase may be considered sufficient to predict the change in the building's dynamic behavior without an unnecessary increase in the number of simulations. However, an additional 15º wind angle is considered to adjudge the adequacy of a 30º increment in the wind incidence., The rest of the study is carried out at an interval of 30º observing insignificant deviations in the results of the 15º wind angle.

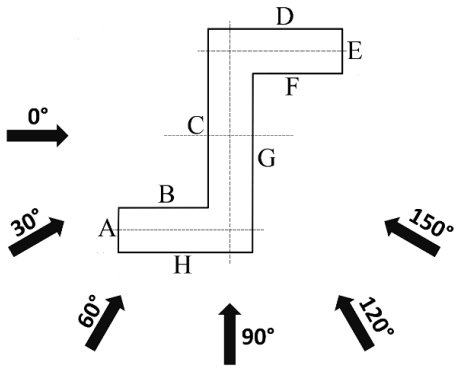

Fig. 9 Definition of the building surfaces and wind angles considered for the study

4.1 Wind flow patterns under different wind incidence angles

The wind flow configuration near the building corresponding to several wind attacks is shown in Fig. 10. The wake region's length and vortices' nature is dependent on the wind angle and the building's geometry. As the building is asymmetric concerning both axes under all considered wind angles, apparently the generated vortices are asymmetric in the wake region too. The flow separation characteristics and vortex generation mechanism at the wake region are understandable from the streamlines and can be referred to justify the peak suctions and pressures obtained at different facets of the building.

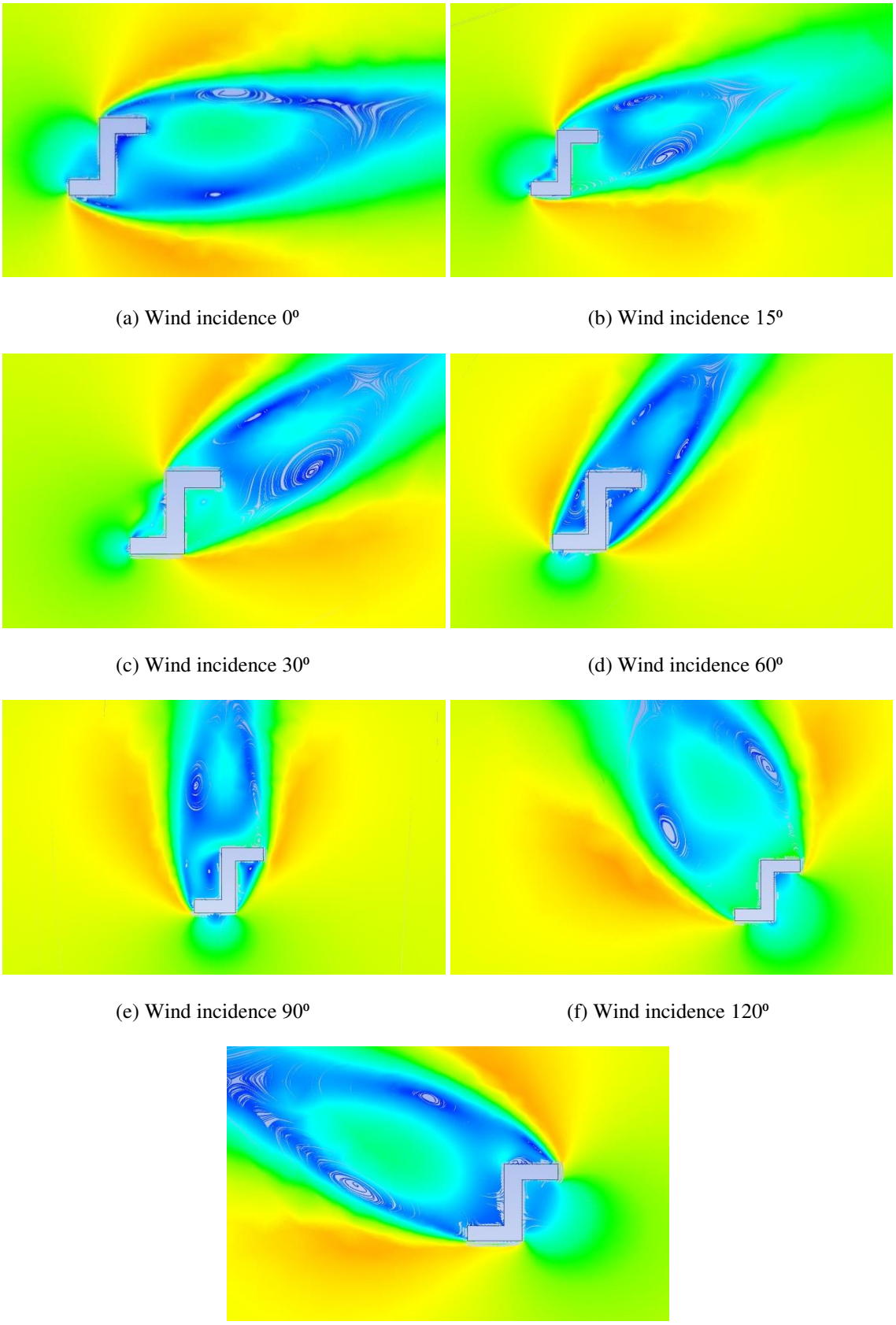

(a) Wind incidence 0º

(b) Wind incidence 15º

(c) Wind incidence 30º

(d) Wind incidence 60º

(e) Wind incidence 90º

(f) Wind incidence 120º

(g) Wind incidence 150º

Fig. 10 Wind stream configuration near the building under varying wind angles

4.2 Peak coefficients and power spectra of wind pressure at building facets

The pressure coefficients are determined. The largest peak pressure coefficient for 0º and 90º wind incidence angles are presented in Fig. 11 (a). The largest peak pressure for Face A is 3.02. There is no pressure on Face D, Face E and Face H under 0º WAA. Being the leeward faces, there is no pressure for Face A to Face E under a wind angle of 90º. Similarly, the least suction coefficients are determined corresponding to 0º and 90º WAA and are presented in Fig. 11 (b). It is seen that; the least suction coefficient is having the minimum value of -3.70 for Face E under 0º wind occurrence angle. At 0º WAA, there is no suction on Face B but even though both Face F and Face G are leeward faces, certain values of peak pressure are obtained. This implies high fluctuation in the pressure due to vortex generation in the region of disturbed flow and separation of flow. Again Face A and Face C are windward faces under 0º WAA but a certain suction value is acquired due to the same reason.

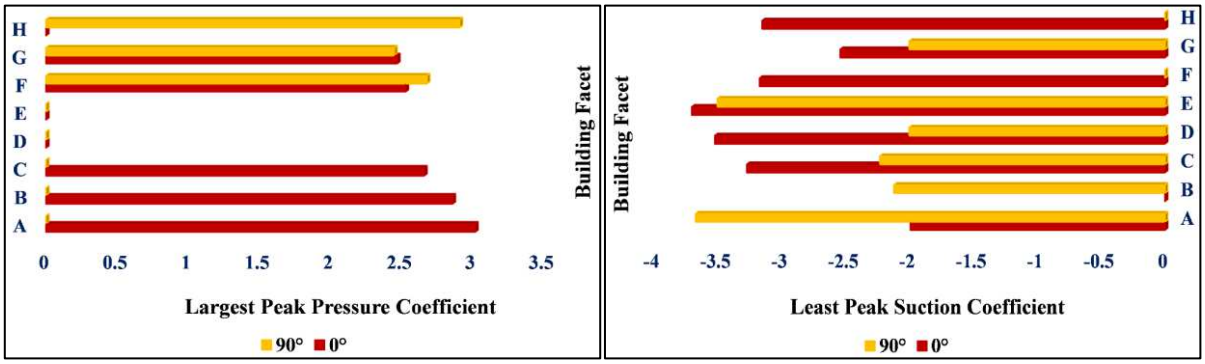

(a) **(b)**

Fig. 11 Peak coefficients at different building facets (a) Pressure; (b) suction

The transient vibration of tall buildings under wind is random because it is motion at many frequencies simultaneously. Fast Fourier Transforms (FFT) are proficient at analyzing vibration in the case when governing frequency components are restricted. Whereas, power spectral density (PSD) plots are expedient in characterizing arbitrary vibration signals. In this study, PSD for the fluctuating pressure in the turbulent flow is derived. A power spectral density plot is derived by multiplying the individual frequency bin in a Fast Fourier Transform by its complex conjugate, resulting in the real only spectrum having a unit of energy per frequency. Normalized power spectra of fluctuating wind pressure consisting $\frac{nS_p(n)}{\sigma_p^2}$ along y-axis and $\frac{n\mathrm{D}}{U}$ (reduced frequency) along the x-axis

are plotted at three different levels of the building concerning different building facets. Where n = vibration frequency in Hz. $S_p(n)$ = the power spectral density in Pa^2/Hz. σ_p^2 = the variance of wind pressure in Pa^2. U = the gradient wind speed in m/s and D = the characteristics width perpendicular to the wind flow in m.

The characteristics of normalized power spectra of wind pressure at the building's top part for various faces subjected to wind azimuths range from 0º to 150º are shown in Fig. 12. The reduced frequency at the peak value of $n_c = \frac{nD}{U}$ where vortex shedding energy is intense, the standardized power spectra can be determined for each case. The first peak is usually occurring in the low-frequency range, where the energy is also relatively lower. But at the top part of the building, some faces are subjected to a second peak at a comparatively high-frequency range. The energy in high frequency increases with the increase in height [29]. For Face E, there is a second peak corresponding to a 90º wind angle of attack at a high value of reduced frequency $n_c = 0.595$, whereas for Face F, the second peak occurs at $n_c = 0.195$ for the same wind angle. Again, for Face G and Face H, the energy increases at a high reduced frequency of 0.125 and 0.210, respectively. For Face G and Face H, the guiding wind angle of attack is 0º. The n_c values concerning the second peaks are marked in the corresponding figures.

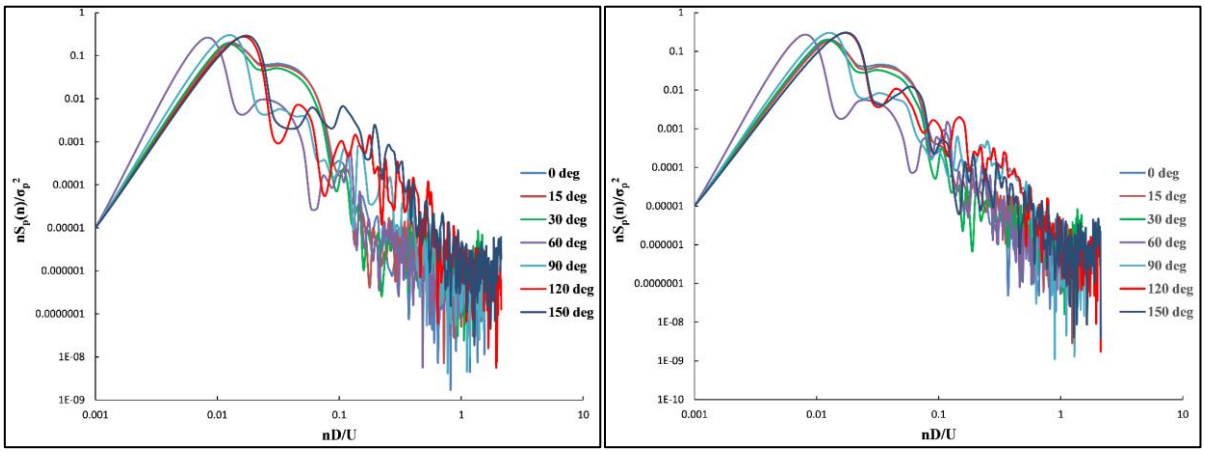

Facet A Facet B

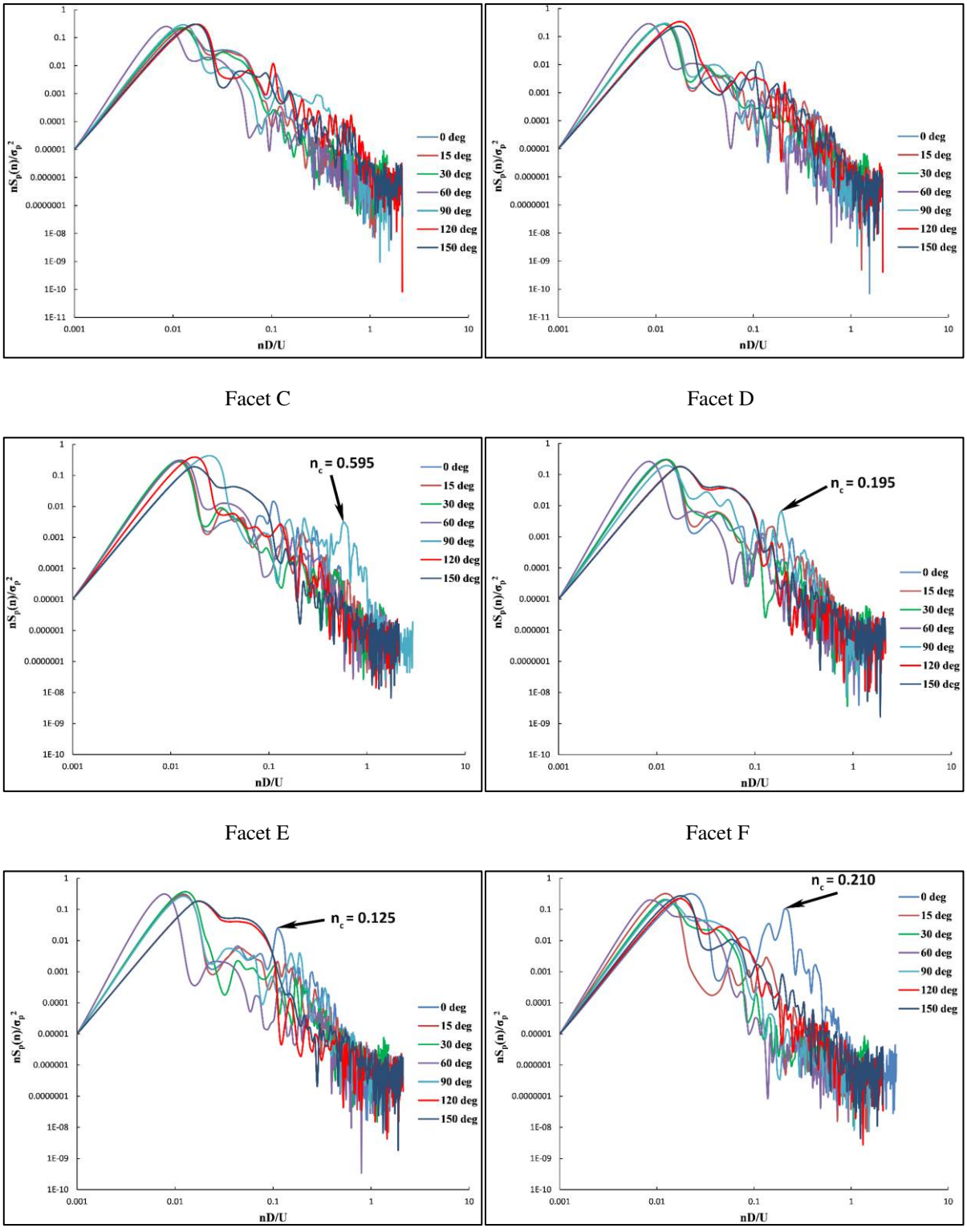

Facet C Facet D

Facet E Facet F

Facet G Facet H

Fig. 12 PSD of building surfaces at the top part against various wind incidence angles

The standardized power spectra of wind pressure at the building's main body for different facets subjected to wind incidence range from 0º to 150º are shown in Fig. 13. The first peak is typically happening at the low frequencies where the energy is also comparatively lesser for all the building facets. However, likewise the top part of the building, some faces are also subjected to a second peak at reasonably high frequencies for the main body. Referring to Fig. 12, for Face C, corresponding to $n_c = 0.110$, the vortex shedding energy increases, and a peak value is obtained for 120º wind angle. In Face D, like all other faces, the primary frequency is low, but there is a second peak corresponding to both 0º and 15º wind incidence angles. The reduced frequency is having a value of 0.185. For Face F, Face G, and Face H, at wind angle 0º, the energy increases at a high-frequency range corresponding to n_c values of 0.115, 0.155, and 0.155, respectively, and a peak is obtained in the power spectra.

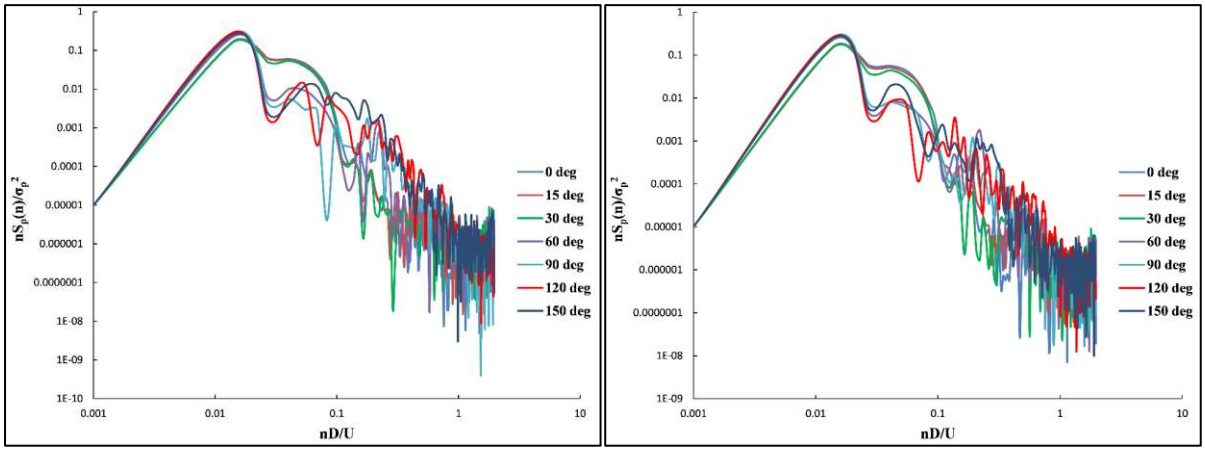

Facet A Facet B

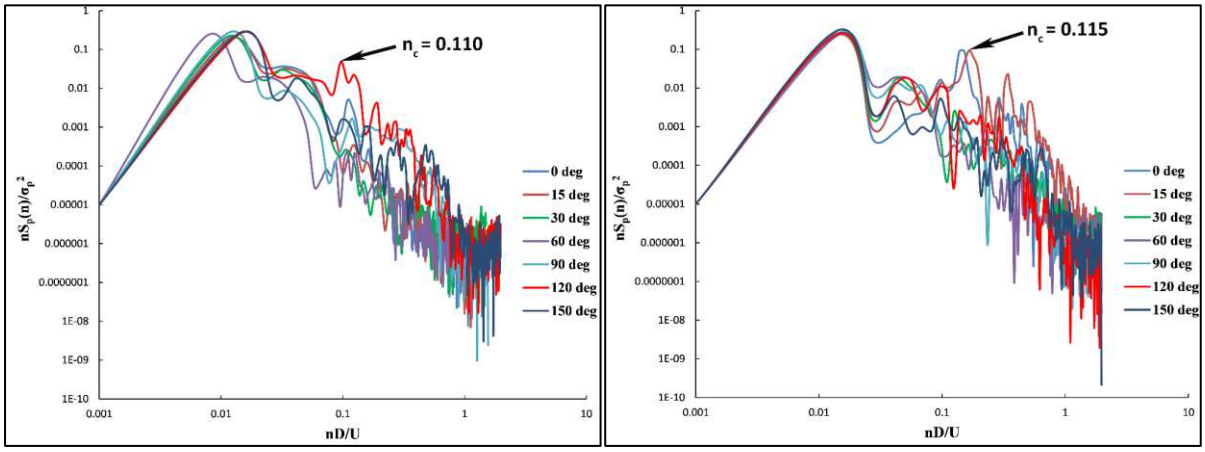

Facet C Facet D

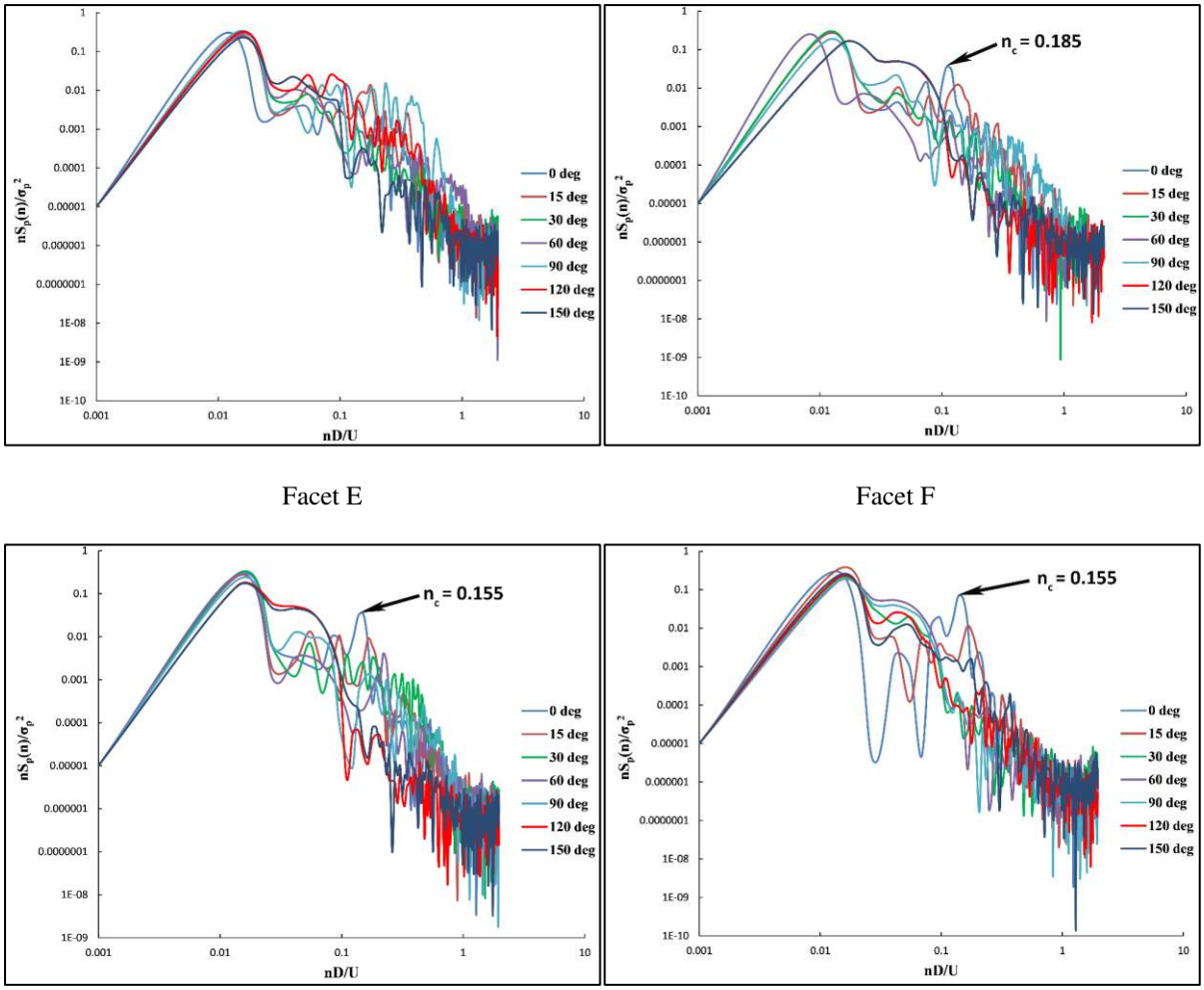

Fig. 13 PSD of building surfaces at the main body against various wind incidence angles

The normalized power spectra of wind pressure at the bottom part of the building are shown in Fig. 14. For the bottom part of the building, it is observed that the peak values of standardized power spectra usually occur in the low-frequency range. Therefore, enhanced vortex shedding energies are also obtained at relatively lower reduced frequencies (n_c) for all the faces. Unlike the top part and main body of the building, most faces are not subjected to a second peak at a relatively high frequency. However, Only Face D and Face H produces prominent second peaks, the energy increases at comparatively high n_c values of 0.12 and 0.028, respectively. Thus it may be stated that for Face H, the second peak under 0^0 wind angle also occurs at a low reduced frequency.

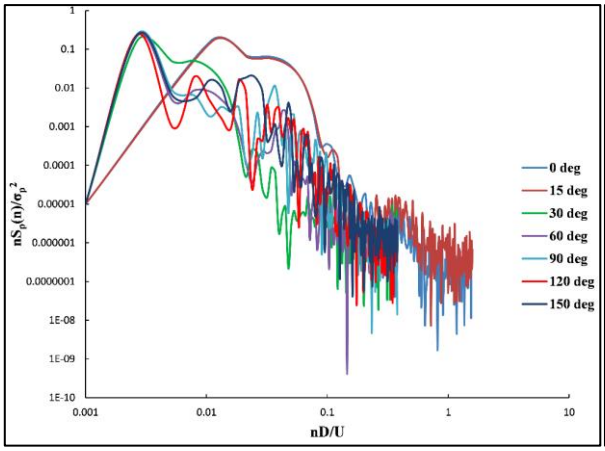

Facet A

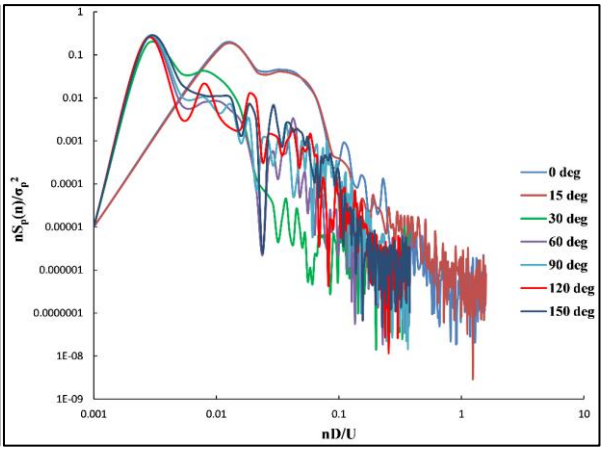

Facet B

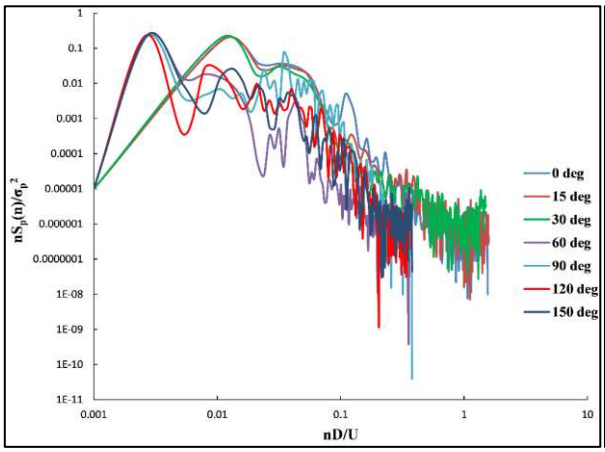

Facet C

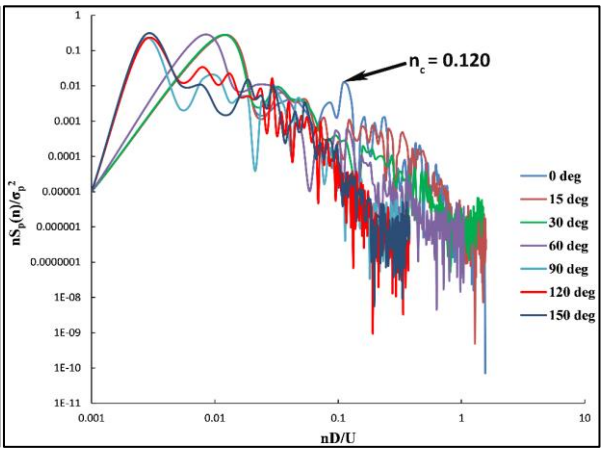

Facet D

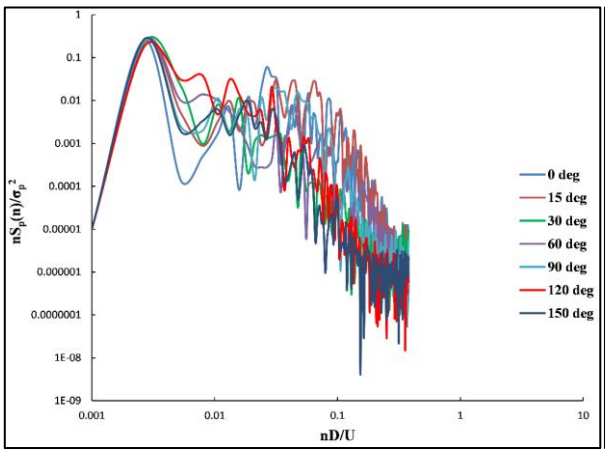

Facet E

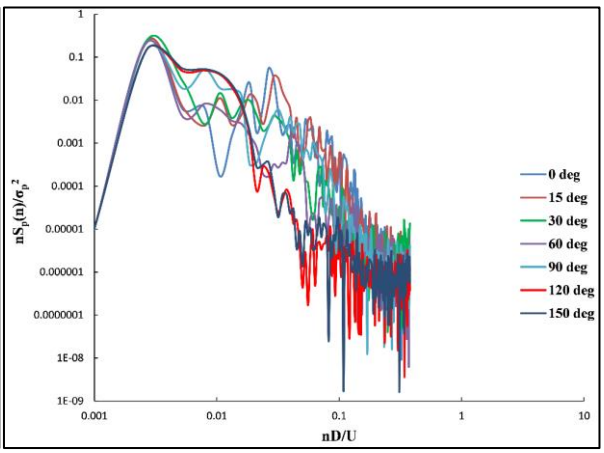

Facet F

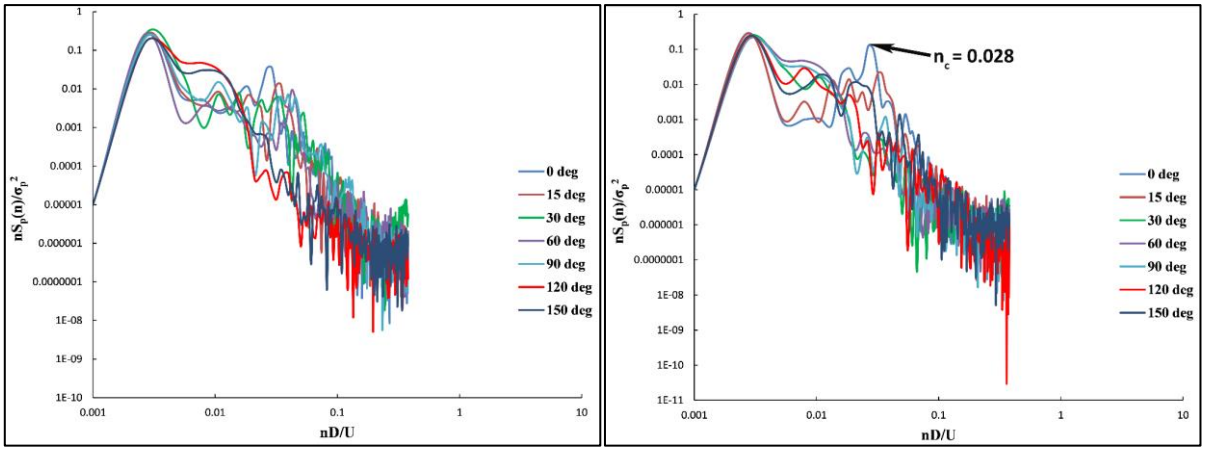

Facet G Facet H

Fig. 14 PSD of building surfaces at the bottom part against various wind incidence angles

6. Conclusions

The building shape considered for the present study is having a rectangular main body with wings on opposite sides. Understandably, the building shape is one of the key factors in reducing the dynamic responses due to turbulent wind speed and transient wind behaviour. Based upon the study of dynamic-wind characteristics and observing the power spectra of wind pressure on various facets of a tall building 'Z' shaped in plan, some concluding remarks can be derived. Firstly, the present study confers that for tall buildings, especially having many corners in the plan shape, wind-structure interaction produces dynamic responses like galloping, flutter, buffeting, and vortex shedding. These vital responses can not be considered explicitly in the quasi-static method of analysis described in wind standards. Hence model analysis is recommended by IS 875 (Part 3): 2015 to get a deeper insight into the phenomenon. Secondly, in the present study, the essential boundary conditions like turbulence intensity and velocity profile upstream of an octagonal building in a wind tunnel are compared with a virtual domain created by CFD. Excellent matches are observed, and it can be concluded with confidence that CFD can suitably be used as a replacement for the experimental method for wind analysis of tall building models. Thirdly, the wind streamlines' characteristics in the plan under the considered wind angles are demonstrated in the study. The flow separation features, nature, and size of generated vortices at the wake region are evident from the streamlines. The probable building facets experiencing wind suction or pressure are perceivable from the flow features. The largest positive and least negative peak pressures corresponding to 0º and 90º WAA are presented. Suction at the windward faces and pressure at the leeward faces may be obtained due to high fluctuation in pressure because of vortex shedding and flow separation under dynamic wind behaviour. Fourthly, the power spectra of

wind pressure against reduced frequency are presented for separate building facets. The resonance phenomenon can be avoided by obtaining the vortex shedding frequencies from the power spectra. Concerning the power spectra at the top part of the building, the first peak in all the building facets occurs at low frequency and low energy. Some surfaces are subjected to a second peak at a relatively high reduced frequency. Building Face E, F, G, and H are experiencing a second peak at a reduced frequency of 0.595, 0.195, 0.125, and 0.210, respectively. The primary peak of the power spectra at the building's main body is typically observed at low frequencies. However, likewise the top part of the building, some faces are also subjected to a second peak at reasonably high frequencies for the main body. A second peak is observed at Face C, D, F, G, and H corresponding to reduced frequency of 0.110, 0.185, 0.115, 0.155, and 0.155, respectively. Enhanced vortex shedding energies are obtained at relatively lower reduced frequencies for all the faces at the bottom of the building. However, Only Face D and Face H produces prominent second peaks at reduced frequency values of 0.12 and 0.028. Therefore, finally, it may be concluded that the vortex shedding energy intensifies under some of the wind angles at the high-frequency range for the top part and main body of the building. However, the vortex shedding energy is lower at a higher value of reduced frequency for the bottom part.

References

[1] IS: 875 (Part-3), *Code of practice for the design loads (Other than Earthquake) for buildings and structures (Part-3, Wind Loads)*, New Delhi, India, 2015.

[2] CWE-92: *Computational Wind Engineering I*, editor, S. Murakami, Elsevier Science BV, 1993.

[3] CWE-96: *Computational Wind Engineering II*, editor, R.N. Meroney and B. Bienkiewicz, Elsevier Science BV, 1997.

[4] A. Kareem, "Lateral-Torsional Motion of Tall Buildings to Wind Loads," *Journal of Structural Engineering, ASCE.* **111**, pp. 2749-2496, 1985.

[5] A. Kareem, "The effect of Aerodynamic interference on the dynamic response of prismatic structures, "*Journal of Wind Engineering and Industrial Aerodynamics.* **25**, pp. 365-372, 1987.

[6] P. J. Saathoff, and W. H. Melbourne, "The generation of peak pressures in separated/reattaching flows. "*Journal of Wind Engineering and Industrial Aerodynamics.* **32**, pp. 121-134, 1989.

[7] T. Stathopoulos, and P. Saathoff, "Wind pressure on roofs of various geometries." *Journal of Wind Engineering and Industrial Aerodynamics.* **38**, pp. 273-284, 1991.

[8] W. H. Melbourne, "Turbulence and the leading edge phenomenon." *Journal of Wind Engineering and Industrial Aerodynamics.* **49**, pp. 45-63, 1993.

[9] D. Surry, and D. Djakovich, "Fluctuating pressures on models of tall buildings." *Journal of Wind Engineering and Industrial Aerodynamics.* **58**, pp. 81-112, 1995.

[10] T. Kijewski, and A. Kareem, "Dynamic Wind Effects: A Comparative Study of Provisions in Codes and Standards with Wind Tunnel Data," *Wind and Structures.* 2001.

[11] S. Liang, Q.S. Li, S., Lui, L. Zhang, and M. Gu, "Torsional dynamic wind loads on rectangular tall buildings," *Engineering Structures.* **26**, pp. 129-137, 2004.

[12] N. Lin, C. Letchford, Y. Tamura, and B. Liang, "Characteristics of Wind Forces Acting on Tall Buildings, "*Journal of Wind Engineering and Industrial Aerodynamics*. **93**, pp. 217–242, 2004.

[13] T. Balendra, M. P. Anwar, and K. L. Tey, "Direct Measurement of Wind-tempted Displacements in Tall Building Models Using Laser Positioning Technique," *Journal of Wind Engineering and Industrial Aerodynamics*. **93**, pp. 399-412, 2005.

[14] M. Gomes, A. Rodrigues, and P. Mendes, "Experimental and numerical study of wind pressures on irregular-plan shapes," *Journal of Wind Engineering and Industrial Aerodynamics.* **93**, pp. 741–756, 2005.

[15] P. Irwin, "Bluff body aerodynamics in wind engineering," *Journal of Wind Engineering and Industrial Aerodynamics*. **96**, pp. 701-712, 2007.

[16] J. Y. Fu, Q. S. Li, J. R. Wu, Y. Q. Xiao, and L.L Song, "Field measurements of boundary layer wind characteristics and wind-tempted responses of super-tall buildings," *Journal of Wind Engineering and Industrial Aerodynamics*. **96**, pp. 1332-1358, 2008.

[17] Y. Kim, K. You, and N. Ko, "Across-wind Responses of an Aeroelastic Tapered Tall Building," *Journal of Wind Engineering and Industrial Aerodynamics*. **96**, pp. 1307-1319, 2008.

[18] A. Zhang, M. Gu, "Wind tunnel tests and numerical simulations of wind pressures on buildings in staggered arrangement," *Journal of Wind Engineering and Industrial Aerodynamics*. **96**, pp. 2067-2079, 2008.

[19] K. C. S. Kwok, P. A. Hitchcock, and M. D. Burton, "Perception of Vibration and Occupant Comfort in Wind Excited Tall Buildings," *Journal of Wind Engineering and Industrial Aerodynamics*. **97**, pp. 368-380, 2009.

[20] K.T. Tse, P.A. Hitchcock, K.C.S. Kwok, S. Thepmongkorn, and C.M. Chan, "Economic perspectives of

aerodynamic treatments of square tall buildings," *Journal of Wind Engineering and Industrial Aerodynamics*. **97**, pp. 455–467, 2009.

[21] M. Gu and Z. N. Xie, "Interference effects of two and three super-tall buildings under wind action," *Acta Mechanica Sinica*. **27**, pp. 687–696, 2011.

[22] N.K. Bhatnagar, P.K. Gupta, and A.K. Ahuja, "Wind pressure distribution on Low –Rise building with Saw- Tooth Roof," *IV National Conference on Wind Engineering*, 2012.

[23] J.A. Amin, and A.K. Ahuja, "Effects of side ratio on wind-tempted pressure distribution on Rectangular Buildings," *Hindawi Publishing Corporation, Journal of Structures*. (Article ID **176739**, 12 pages), 2013.

[24] S.K. Verma, A.K. Ahuja, and A.D. Pandey, "Effects of wind incidence angle on wind pressure distribution on square pan tall buildings," *Journal of Academic Industrial Research*. **1**, pp. 747–752, 2013.

[25] R.T. Muehleisen, and S. Patrizi, "A new parametric equation for the wind pressure coefficient for low-rise buildings," *Energy and Buildings*. **57**, pp. 245-249, 2013.

[26] T. Kushal, A.K. Ahuja, and A. Chakrabarti, "An experimental Investigation of Wind Pressure Developed in Tall Buildings for different plan Shape," *International Journal of Innovative Research & Studies*. **1**, pp. 605–614, 2013.

[27] A.K. Dagnew, and G.T. Bitsuamlak, "Computational evaluation of wind loads on a standard tall building using LES," *Wind and Structures*. **18**, pp. 567-598, 2014.

[28] F. Sun, and M. Gu, "A numerical solution to fluid-structure interaction of membrane structures under wind action," *Wind and Structures*. **19**, pp. 35-58, 2014.

[29] D.M. Huang, L.D. Zhu, and W. Chen, "Power spectra of wind forces on a high-rise building with section varying along height," *Wind and Structures*. **18**, pp. 295-320, 2014.

[30] B. Bhattacharyya, S.K. Dalui, and A.K. Ahuja, "Wind induced pressure on 'E' plan shaped tall buildings," Jordon Journal of Civil Engineering. **8**, pp. 120–134, 2014.

[31] L. Zhi, B. Chen, and M. Fang, "Wind load estimation of super-tall buildings based on response data, "*Structural Engineering and Mechanics*. **56**, pp. 625-648, 2015.

[32] R. Paul, and S.K. Dalui, "Wind effects on 'Z' plan-shaped tall building: a case study," International Journal of Advanced Structural Engineering. **8**, pp. 319-335, 2016.

[33] P. Sanyal, and S.K. Dalui, effect of courtyard and opening on a rectangular plan shaped tall building under wind load, " *International Journal of Advanced Structural Engineering*. **10**, pp. 169-188, 2018.

[34] Y. Li, X. Tian, K.F. Tee, Q.S. Li, Y.G. Li, "Aerodynamic treatments for reduction of wind loads on High-rise Building," *Journal of Wind Engineering and Industrial Aerodynamics*. **172**, pp. 107-115, 2018.

[35] M. Mallick, and A. Mohanta, "Prediction of Wind-tempted Mean Pressure Coefficients Using GMDH Neural Network," *Journal of Aerospace Engineering*, **33,** pp. 1-17, 2019.

[36] A.K. Bairagi, and S.K. Dalui, "Forecasting of Wind Induced Pressure on Setback Building Using Artificial Neural Network," *Periodica Polytechnica Civil Engineering*, **64**, pp. 751-763, 2020.

[37] R. Paul, and S.K. Dalui, "Prognosis of Wind-Tempted Mean Pressure Coefficients of Cross-Shaped Tall Buildings Using Artificial Neural Network," *Periodica Polytechnica Civil Engineering*, **64**, pp. 1124-1143, 2020.

[38] R. Paul, and S.K. Dalui, "Optimization of alongwind and crosswind force coefficients on a tall building with horizontal limbs using surrogate modelling," *Structural Design of Tall and Special Buildings*, **30**, pp. 1-20, 2021.

[39] R. Paul, and S.K. Dalui, "Shape Optimization to Reduce Wind Pressure on the Surfaces of a Rectangular Building with Horizontal Limbs," *Periodica Polytechnica Civil Engineering*, **65**, pp. 134-149, 2020.

[40] Recommended practice, DNV-RP-C205, Environmental conditions and environmental loads, Høvik, Norway, 2010.

[41] J. Revuz, D.M. Hargreaves, and J.S. Owen, "On the domain size for the steady-state CFD modelling of a tall building," *Wind and Structures*. **15**, pp. 313–329, 2012.

[42] SK. Dalui, "Wind Effects on Tall Buildings with Peculiar Shape," Roorkee: (Doctoral Dissertation), Retrieved from Indian Institute of Technology, Roorkee Database, 2008.

[43] AS/NZS 1170.2:2021, Australian/New Zealand Standard. Structural Design Actions, Part 2: Wind Actions, Sydney, NSW, Australia and Wellington, New Zealand, 2021.

[44] ASCE STANDARD (ASCE/SEI 7-16). Minimum Design Loads for Buildings and Other Structures, Reston, Virginia, USA, 2016.